cycloTRACK (v1.0) - Tracking winter extra-tropical cyclones based on relative vorticity: Sensitivity to data filtering and other relevant parameters

Emmanouil Flaounas (1), Vassiliki Kotroni (2), Konstantinos Lagouvardos (2), Ilias Flaounas (3)

1 LMD/IPSL, CNRS and Ecole Polytechnique, Palaiseau, France

2 Institute for Environmental Research and Sustainable Development, National Observatory of Athens, Athens, Greece

3 Intelligent Systems Laboratory, University of Bristol, Bristol, UK

Abstract

In this study we present a new cyclone identification and tracking algorithm, cycloTRACK. The algorithm describes an iterative process. At each time step it identifies all potential cyclone centers, defined as relative vorticity maxima embedded in smoothed enclosed contours of at least $3x10^{-5}$ s^{-1} at the atmospheric level of 850hPa. Next, the algorithm finds all the potential cyclone paths by linking the cyclone centers at consecutive time steps and selects the most probable track based on the minimization of a cost function. The cost function is based on the average differences of relative vorticity between consecutive track points, weighted by their distance. Last, for each cyclone, the algorithm identifies “an effective area” for which different physical diagnostics are measured, such as the minimum sea level pressure and the maximum wind speed. The algorithm was applied to the ERA-Interim reanalyses for tracking the northern hemisphere extra-tropical cyclones of winters from 1989 until 2009 and we assessed its sensitivity for the several free parameters used to perform the tracking.

1. Introduction

Identification and tracking of atmospheric features is an active area of research. Examples of recent works include the Mesoscale Convective Systems (MCS; e.g. Machado et al, 1998), the conveyor belts (e.g. Eckhardt et al, 2004), the cut-off lows (Wernli and Sprenger, 2007), the fronts (Hewson and Titley, 2010), the jet streams (Limbach et al, 2012) and the dry air intrusions (Roca et al, 2005; Flaounas et al, 2012). However, the most investigated atmospheric features targeted by identification and tracking algorithms are the tropical and extra-tropical cyclones (e.g. Hodges, 1999; Blender and Schubert, 2000; Hoskins and Hodges 2002; Ulbrich et al, 2009; Inatsu, 2009).

The typical methods for cyclone detection and tracking follow a two-step approach. First, they identify the locations of cyclone centers at each time step and then the cyclones paths are extracted by connecting the centers of consecutive time steps. During the identification step, several constraints are applied in order to control the range and the number of the identified features. For example, in some studies, the definition of the location of a cyclone implies three constraints on the fields of mean sea level pressure: (1) the representative grid point of the data field has to have the minimum value among the adjacent grid points; (2) the minimum value has to be inferior of a threshold value; and (3) the field gradient has to be superior of a threshold value (e.g. Murray and Simmonds, 1991; Blender and Schubert, 1997; Nissen et al, 2010). However, there is a trade off. The application of such “strict” constraints on pressure gradients may lead to tracking cyclones only during their mature stage and furthermore, weak cyclones may be left undetected.

An efficient cyclone tracking algorithm has to be able to decide if the identified features have moved over time or if they have ceased to exist. An extra challenge is that cyclones can split or even merge with other cyclones. Also, there might exist more than one candidate location to be considered as the next cyclone center. This is the case of noisy fields, where a significant number of grid points, typically located close to each, can be considered as cyclone centers. The algorithm has to determine automatically which of the candidate features should be tracked and which should be neglected. Many methods apply an across time “nearest neighborhood” approach where tracks are built by connecting the identified cyclone centers of one time step with the nearest neighbors of the following time step (Blender et al., 1997; Serreze et al., 1997; Trigo et al., 1999). Other studies use more complex tracking

algorithms based on displacement speed (e.g. Murray and Simmonds, 1991; Wernli et al, 2006; Davis et al, 2008; Campins et al, 2011; Hanley and Caballero, 2012). These algorithms make a “guess” on the next step location of the cyclone and choose the nearest feature detected at that potential location. Finally, Inatsu (2009) presented an algorithm where cyclones are identified as areas of enclosed grid points that satisfy a certain condition on filtered meridional wind at 850 hPa. Then, cyclone tracking is performed by connecting the cyclone areas that overlap in consecutive time-steps

Hodges (1999) proposed a post-processing of the identified features and their tracks. His method starts by building all potential tracks using the nearest neighborhood approach. Then, the identified tracks exchange track points between them until an overall cost function is minimized. This cost function is a measure of the smoothness of the whole set of tracks. Hanley and Caballero (2012) also applied a post-processing approach in order to cover the cases where cyclones that have more than one centers undergo any merging or splitting process.

Raible et al. (2008) were the first to compare the performance of three different tracking methods, applied on extra-tropical cyclones. Their results converged on the interannual variability of cyclone occurrences; however they differed on the cyclone number trends and track densities. Recently the IMILAST project presented a comparison of the performance of 15 different algorithms which have been applied for the tracking of extra-tropical cyclones during the cold season of 21 years over the entire planet (Neu et al, 2013). They found that the number of tracks, the lifetime and the intensity of cyclones may vary significantly depending on the algorithm used. This apparent disagreement of the algorithms can be easily explained by the fact that there is no commonly accepted definition of a cyclone. Consequently, each algorithm applies different constraints and/or different fields. In this sense, one of the main results of Neu et al. (2013) is that no algorithm can be considered to be “superior” or more “correct” than the others, since they use different definitions of a cyclone. However, it is noticeable that even algorithms with similar configurations may present a divergence of results. Recently, Ulbrich et al. (2013) treated the extra-tropical cyclones tracks evolution in the context of a changing climate using a multi tracking methods approach. It was shown that despite the differences on the tracks number, the algorithms present comparable results on the cyclones

climatology future trends. This finding confirms that there is a common robust behavior independently of the different algorithms configurations and modeling constraints.

In this study, our principal motivation was to design an algorithm that is able to provide qualitative characteristics of the features like splitting, merging, wind speed, associated rainfall and minimum pressure, in parallel with the tracking. A new aspect of the proposed approach is that cyclonic features are tracked based on their physical properties by assuring a gradual evolution of the cyclone relative vorticity and not based on their displacement. The use of relative vorticity presents some advantages compared to the use of geopotential height or mean sea level pressure. It is a high frequency variable, representative of local scales that -presumably- permits cyclone tracking at an early stage, i.e. during its initial perturbation and before it is characterized by closed pressure contours (Sinclair, 1994, 1997; Hodges 1999; Inatsu 2009; Kew et al, 2010). This can be an advantage in cases where cyclones intensity increases significantly within 24 hours, i.e., explosive cyclogenesis (e.g. Sanders and Gyakum, 1980; Trigo et al, 2006; Lagouvardos et al, 2007). The disadvantages of relative vorticity is that it is a wind-based field, sensitive to the horizontal resolution of the dataset, and that local maxima might not correspond to wind vortices but to other features such as an abrupt wind turning.

To deal with the spatial noise of relative vorticity, we smooth the input fields. The smoothing operation partly counteracts the property of relative vorticity to detect cyclones in their early stage, however our algorithm has a high degree of flexibility that permits the tracking of perturbations that did not evolve to strong cyclones. Similar approach has been used before in other studies for capturing weak cyclonic features (e.g. Murray and Simmonds, 1991; Pinto et al, 2005), but in our case it provides an additional value on optimizing the algorithm and determining the cyclones that are not sensitive to filtering. The application and assessment of our method is performed in line with the efforts of the IMILAST project. We used the same time periods and input datasets in order to make our results comparable with those of the aforementioned project.

In Section 2 we described in detail cycloTRACK, our cyclone detection and tracking algorithm. In Section 3 we present the results of several sensitivity tests of our method, applied to the ERA-Interim

(ERA-I) data set for the winters (December-January-February) of the period 1989-2009. Finally, Section 4 hosts the conclusions and our prospects for future research.

2. Identification and tracking algorithm

In this section we present our algorithm, cycloTRACK, and its application on the vorticity fields at 850hPa level within the extra-tropical latitudes of the Northern hemisphere during the winters of 1989-2009. We use meteorological data from the 6-hourly ERA-I reanalyses with a horizontal resolution of 1.5°x1.5° (Uppala et al, 2008). The algorithm is composed by two independent steps. In the first step, we identify all cyclonic features for all time steps of a dataset and in the second step we build the cyclone tracks.

2.1 Step-I: Identifying cyclones and quantifying their characteristics

The first step of the algorithm is devoted to the identification of the cyclones and to the quantification of their characteristics. Initially, the algorithm identifies all cyclonic features, or more precisely all cyclonic circulations. Then, for each cyclonic circulation the algorithm identifies the representative centers which will be treated as distinct cyclones. Finally, for each center, the algorithm quantifies its characteristics like the maximum relative vorticity, the maximum wind speed and the minimum sea level pressure.

2.1.1 Identification of cyclonic circulations

To identify cyclonic circulations, the vorticity field is smoothed by applying a spatial filter. In previous studies the vorticity field has been smoothed by a variety of filtering operations like for example b-spline techniques (Hodges, 1995), time band-pass filtering (Hoskins and Hodges, 2002; Inatsu, 2009) and 1-2-1 filters (Satake et al, 2013). In this study, we use the simple method of a 1-1-1 spatial filter,

which smoothes efficiently the orographic or the coastal vorticity maxima and the gradients of relative vorticity fields. The latter also helps the algorithm to reject local vorticity maxima that are nested within noisy field gradients – especially when considering very high resolution datasets. The smoothing operation on the relative vorticity field is performed at each grid point separately by multiplying the sum of all its adjacent grid points within distance X by 1/(2X+1). For instance, at any grid point (a, b) the smoothed Relative Vorticity (RV) is given by:

$$RV_{a,b} = \frac{1}{(2X+1)^2} \cdot \sum_{i=a-X}^{a+X} \sum_{j=b-X}^{b+X} (RV_{i,j}) \qquad \text{Eq. 1}$$

As X increases, the smoothing operation on the relative vorticity field becomes stronger. Finally, we apply a threshold and we retain only the grid points exceeding this threshold.

Figure 1 shows the raw relative vorticity fields and the corresponding fields after the application of three different filters with 2X+1 equal to 3, 5 and 7. The relative vorticity fields are derived from ERA-I and are centered over Europe at 00:00 UTC, 3 December 1999, featuring the Anatol storm over Denmark as the strongest detected cyclone. In all panels of Fig. 1 the threshold is set to $3x10^{-5}$ s^{-1}. As the applied filter becomes stronger, the relative vorticity values become weaker. Small vorticity features tend to be suppressed, however the structure and location of the vorticity maxima of the strongest features, such as the Anatol storm, are not altered among the different filter operations. We used filtering for smoothing the values within a cyclonic circulation. Thus, the filtering matrix should not be much larger than the length scale of a cyclone. In this sense, a 7x7 grid point filter for ERA-I means that relative vorticity is smoothed over a 10.5°x10.5° region which is certainly a large area.

As shown in Figs 1a and 1b, each cyclonic circulation might correspond to a unique cyclone or to a large complex of cyclonic centers comprised by more than one local maximum. The $3x10^{-5}$ s^{-1} threshold applied on the ERA-I dataset (1.5°x1.5° resolution) has been found adequate for describing cyclones even at their initial stage, for all three filtering sensitivity tests. In this step, the algorithm identifies and labels with a number all cyclonic circulations which are defined as the areas composed by neighboring grid points of values exceeding the $3x10^{-5}$ s^{-1} threshold. The threshold value allows

tuning the algorithm for detecting cyclones in coarse resolution datasets (e.g. 1.5°x1.5°, as in ERA-I used here) or in high resolution datasets (e.g. 20km regional climate runs). Applying a threshold is a convenient approach for adjusting the filtering strength. Alternatively, we could keep the filtering strength constant and allow the threshold value to vary. However, it is only by varying the filtering strength that the vorticity field may be smoothed within the characteristic length scale of cyclones. Similar approaches of identifying a feature through an enclosed area have been used before for cyclones (e.g. Hodges 1999; Wernli et al, 2006; Inatsu, 2009; Flaounas et al 2013) and for MCS (e.g. Machado et al, 1998).

2.1.2 Identification of cyclonic centers

A careful inspection of Figure 1b, 1c and 1d reveals that the cyclonic circulations do not correspond to the same cyclone. For this reason each labeled cyclonic circulation is further treated in order to locate all embedded local vorticity maxima. These local maxima will be labeled and eventually they will be treated as centers of unique cyclones. The term “centers of unique cyclones” has no physical basis but it is conveniently used here in order to describe the grid points that present local maxima of relative vorticity and that we follow in time in order to construct cyclones tracks. In this sense we need to provide the algorithm with a representative cyclone center even though the cyclone structure might be very complex with more than one vorticity maximum (especially in very high resolution datasets). To deal with this issue (1) we filter the data, smoothing the noisy gradients (already performed in the previous step); (2) we define the local maximum as the maximum value of the central grid point among its eight surrounding grid points; and (3) we consider that between two centers there is a relative vorticity difference greater than a threshold value (in this case set equal to $3x10^{-5}$ s^{-1}) which is applied to define the cyclonic circulations. The last criterion prohibits weak cyclonic circulations, i.e. cyclones of relative vorticity close to the threshold value, to present multiple centers.

2.1.3 Quantifying cyclone characteristics

Once all cyclones have been identified, we determine an “effective area” for each cyclone. This area is a circular disk centered at the cyclone vorticity maximum. The disk radius grows gradually until: (1) all grid points included in the disk have a vorticity average inferior to a threshold value; or (2) the radius reaches a pre-defined maximum length; or (3) a relative vorticity value greater than that of the cyclonic center, is found within the area. According to this empirical method, the strong or the large and weak cyclones tend to produce large effective areas. The third criterion favors the stronger cyclones to spread their area independently of the presence of other weaker ones in their region, while it restrains the weaker cyclones to share the same area with stronger cyclones. In Flaounas et al. (2013) the cyclone area was defined by the cyclone enclosed contour as defined by the applied threshold value (see their appendix figure). However, such an enclosed area might not capture grid points that present relative vorticity values lower than the applied threshold. In Lim and Simmonds (2007) the cyclone area was defined by a representative circular disk of radius equal to the average distance between the cyclone center and the enclosing zero contour of the mean sea level pressure laplacian. The circular disk seemed to be the best choice for our algorithm in order to capture the areas affected by a cyclonic vortex. Irregular shapes may also be considered, as for instance enclosed contours of pressure (Wernli et al, 2006; Hanley and Caballero, 2012) or relative vorticity (Flaounas et al, 2013).

Once the effective area is defined, our algorithm computes the physical properties of the cyclone within it. Figure 2 shows as an example the effective area and the detected minimum sea level pressure and maximum 10-meter wind of the storm Anatol at the same time as in Figure 1b.

2.2 Step-II: Tracking cyclones

In this step we combine the cyclone centers into a track. First, the algorithm sorts the identified cyclones based on their relative vorticity value, from the strongest, i.e., the one with the highest relative vorticity value, to the weakest. Then, it starts from the first cyclone and searches forward and backward in time for all its possible tracks. More precisely, the algorithm constructs all possible

cyclone tracks that share the same the maximum vorticity track point. Once all possible tracks are constructed, the algorithm chooses the track that presents the most “natural evolution” of relative vorticity, i.e., the track which presents the smallest differences of relative vorticity in consecutive points, weighted by the distance between the track point locations.

Figure 3a illustrates an idealized experiment, presenting the locations of all identified cyclones in a four time steps dataset. Six cyclones are identified: one in the first time step, one in the second time step and two for time steps three and four. The tracking process begins from the strongest cyclone (i.e., the cyclone 2(12)) and constructs all possible tracks by iterating forward and backward in time with all other features. Figure 3b shows that the first cyclone may undertake four possible tracks, however it is obvious that the track 1(9), 2(12), 3(10), 4(8) presents the most “natural evolution”, since maximum relative vorticity presents the smallest difference from one time step to the next. The algorithm saves this track and deletes the used cyclones’ locations from the dataset. Then, a new iteration begins where the algorithm will start from the cyclone with the highest vorticity and eventually a new track will be constructed (Figure 3c). We found that starting the tracks from the cyclone’s mature state is more efficient for the construction of the first steps of the tracks. Indeed, for most cases in the previous and in the following time step of the cyclone with the highest vorticity state, there is only one strong cyclone to act as a candidate for continuing the tracks.

The practice of cost function minimization has been used in relevant literature of tracking algorithms. Hodges (1995) built the feature tracks by minimizing the cost function of the feature’s track smoothness, while Hewson and Titley (2010) built the feature tracks by applying a likelihood score on its physical characteristics. Our cost funcrion measures the absolute average difference of the relative vorticity weighted by the distance between two consecutive time steps:

$$C = \frac{\sum_{n=1}^{n=N-1} d_{n \to n+1}\left(\left|V_{n+1} - V_n\right|\right)}{\sum_{n=1}^{n=N-1} d_{n \to n+1}} \qquad \text{Eq. 2}$$

Where $\boldsymbol{C}$ is the cost function of a candidate track, $\boldsymbol{N}$ is the total number of the track's time steps, $\boldsymbol{d}$ is the distance between two consecutive track points and $\boldsymbol{V}$ is the relative vorticity at each time step.

The number of potential tracks is quite large. However, their number can be significantly reduced by the application of a series of legitimate heuristics that remove tracks that present a "non-natural" behavior: (1) the location of the next candidate cyclone must be within a threshold range between successive time steps; (2) the maximum vorticity between the tracked cyclone and a candidate cyclone must not differ by more than 50%; and (3) if the displacement between two successive displacements is more than 3° long, then the angle between these displacements must be greater than 90°. The first constraint prohibits the algorithm from searching for candidate features in the following time step in locations where the tracked cyclone could not be located. In our algorithm the cyclones are searched within a 5°x10° latitude-longitude range. This is the largest possible displacement for extratropical cyclones as proposed by Hodges (1999). The second constraint prohibits the algorithm from choosing candidates that cannot be a possible evolution of the tracked feature. The use of a percentage is highly convenient since large vorticity values are subject to higher changes between consecutive time steps compared to smaller vorticity values. Finally, the third constraint prohibits the algorithm from taking into account a back-and-forth movement of the cyclone. Such displacements are more likely to take place in raw vorticity fields, where local maxima might change abruptly. For example, our algorithm would not choose the track 2(12), 3(4) and 4(8) as presented in Figure 3, since the consecutive displacements present an angle of 74° (marked in red) which is smaller than 90°.

Finally, cycloTRACK returns as output one matrix for each track that contains information on the cyclone's track and its physical characteristics. Each matrix has one row for each of the track points and one column for each of the standard outputs and the optional physical diagnostics. These optional output diagnostics may vary depending on the study and the data inputs. Labeling the cyclonic circulations (section 2.1.1) and the cyclonic centers (section 2.1.2) within the tracks permits a post-processing analysis for determining potential merging and splitting of cyclones. For our application on the extra-tropical cyclones we consider only maximum 10-meter wind speed and sea level pressure minima. Figure 4 presents two cyclone tracks which evolve by sharing the same cyclonic circulation

as an example of the algorithm performance. Using the effective area diagnostic, in Figure 5 we show the evolution of the two cyclones relative vorticity, maximum 10-meter wind speed and minima of sea level pressure.

It is likely that our method detects fronts associated with vorticity maxima as cyclone centers, especially when applied to high resolution datasets, for example regional climatic simulations. In order to avoid the detection of a frontal zone, additional criteria of high or low complexity should be considered (e.g. Hewson and Titley, 2010). However, such criteria could be dependent on several factors – as for instance the spatial resolution of the dataset – and would result to a "stricter" cyclone definition. The more precise the mathematical criteria, the more constrained are the tracking results to systems of specific characteristics. For example, in the case of fronts this could exclude the early stages of certain tracked cyclones that emerge from high vorticity frontal areas of a "parent" cyclone.

Figure 4 illustrates an example of a front detection. Inspection of surface pressure charts (not shown) showed that the first track point of the second cyclone (red dot in Fig. 4b) corresponds to the front of an extra-tropical cyclone (the one depicted by the black track). In the following time steps (Fig 4c to 4f), this secondary vorticity maximum evolves to a strong cyclone (red track) which presents its own low pressure minimum. Here we capture the initial stage of the vorticity maximum, before the occurrence of a pressure minimum. Nevertheless, skipping the application of additional criteria may require a post-processing of the resulting tracks in order to exclude the "wrong" ones or those that do not match the research needs.

3. Application of cycloTRACK in a climatological context and analysis of its sensitivity

In this section we present the results of the application of our algorithm for all winters (December, January and February) of the period 1989-2009. We also present the results on three sets of sensitivity tests: (a) on relative vorticity filtering; (b) on the cost function of Eq. 2; and (c) on the constraint that relative vorticity between two consecutive track points must not differ more than 50%. In all sensitivity tests, the threshold used to define cyclones is $3x10^{-5}$ s^{-1} and we analyze only those tracks

with longer than one day lifetimes.

3.1 Sensitivity on filtering the relative vorticity field

We tested three different filter strengths (described in section 2.1.1) to the ERA-I dataset. The applied spatial filters correspond to a 3x3, a 5x5 and a 7x7 grid points filtering, named as *filter3*, *filter5* and *filter7*, respectively. Figure 6a presents the number of detected cyclonic centers as a function of their relative vorticity for all three sensitivity tests and Fig. 6b their relative frequency. Since all tests are bounded to identify cyclones exceeding a common threshold of $3x10^{-5}$ s^{-1} and since filtering decreases the relative vorticity values due to its smoothing operation, it is of no surprise that the total number of detected cyclone centers is reduced with increasing filtering intensity. Regardless of the spatial filtering strength, all three sensitivity tests present an exponential distribution (Fig. 6a), and the stronger the filter, the more the cyclones intensities are reduced (Fig. 6b).

Strong filtering versus weak filtering may have two effects. First, it tends to detect fewer tracks which also correspond to the stronger cyclones. Second, it tends to reduce the cyclone track lengths by not taking into account the weakest vorticity perturbations in the early and late stages of a cyclone track. The validity of the first hypothesis is evident from Fig. 1 where smoothing suppresses many weak cyclonic centers, but stronger cyclones (such as the Anatol storm) are equally detected with all three filters. To verify the second hypothesis we investigate the characteristics of the tracks as detected by *filter3*, *filter5* and *filter7*. Figures 7a, 7b and 7c show the distribution of the relative frequency for the lifetime of cyclone tracks, the average speed of the cyclones and their maximum relative vorticity. We observed no significant changes on the results obtained with the different filters when considering the cyclone lifetime. Consequently, the second hypothesis, that average track characteristics are sensitive to filtering, can be rejected. It is interesting though that our applications using weak filtering detect weak cyclones that have similar lifetime scales. The distributions of the relative frequencies of average speed of cyclones are similar for all three filters (Fig. 7b). This means that the weaker cyclones in *filter3* and *filter5* do not correspond to weak stationary vorticity perturbations, and they also do not

evolve to strong extra-tropical cyclones. The reasons for not evolving to strong cyclones is an interesting issue, however it is not in the scope of this paper.

Figure 8 shows the Cyclones Center Density (CCD) for all three filtering strengths. It is evident that different magnitudes of CCD are observed that depend on the filtering strength; however, the spatial pattern remains coherent for all three cases. A question that may arise is whether all sensitivity tests share the same cyclone centers, while additional weak centers are detected in *filter3* and *filter5* that are suppressed in *filter7* due to the smoothing operation. To address this question we took into account all points of the distributions in Fig. 6 and we associated the common points between *filter3* and *filter7* (points sharing the same timing and having a distance inferior of 5°). Results showed that *filter7* shared 52% of its points (2331 points) with *filter3*. The median of the intensity of the common points of *filter3* corresponded to the 78^{th} percentile of all *filter3* points' intensity. Consequently, cyclones in *filter7* correspond to the strongest cyclones of the weakly filtered data. This comes in accordance with the relative frequency of cyclone centers intensity in Fig. 6b, where most identified cyclones using *filter7* are concentrated to weaker relative vorticity values, compared to *filter3* and *filter5*.

The effect of filtering, for example *filter7* compared to *filter3*, is characteristic to the CCD within the Mediterranean region, where the cyclones are known to be weaker than the extratropical cyclones forming over the oceans (Campa and Wernli, 2012). Indeed, in *filter7* there is a dramatic decrease of detected cyclones over the Mediterranean Sea compared to *filter3* and *filter5*. Figure 8 presents a high similarity with the results of other algorithms (Neu et al., 2013) independently of whether a filtering was applied or whether the sea level pressure and the relative vorticity were used as inputs for the detection of cyclones. Indeed, CCD maxima are distinctly located over the Pacific Ocean, the Northern Atlantic Ocean, and the Mediterranean. Furthermore, regardless the filtering strength, both cyclone speed and lifetime relative frequency distributions (Figs. 7a and 7b) seem to be in good agreement with the other algorithms (Neu et al, 2013) presenting most probable cyclone speeds between 30 to 40 km/hour and cyclone lifetime relative frequency distributions decreasing exponentially from less than 2 days up to a total of approximately 8 days.

Figure 9 presents the annual number of cyclone centers. For all three filters, our results are in agreement with those of Neu et al. (2013) showing no specific inter-annual trend. As expected, the number of cyclone centers per year depends on the filtering strength. It decreases from approximately 9000/year for *filter3* to approximately 3000/year for *filter7*. All three tests are within the ranges of other algorithms that range from 2000/year to 12000/year. However, it is only *filter5* that is consistent with the majority of the results of other algorithms, which calculated 4000 to 7000 cyclonic centers per year. The time series phasings are in good agreement between *filter3* and *filter5*, presenting a correlation of 0.91. On the other hand, correlation between *filter5* and *filter7* is 0.43, suggesting that the time series phasing between the two sensitivity tests is dependent to the weaker cyclones that are suppressed in filter7. This should not raise a question on the soundness of the different test results, but on the results sensitivity to the different filtering strengths.

3.2 Sensitivity on tracking parameters

We performed two additional sets of sensitivity tests in order to assess the efficiency of our tracking method (Step-II). The first set relates with the cost function (Eq. 2) and it is composed by: (a) S_{rel}, where the final track choice in step-II is only dependent to the track relative vorticity evolution (Eq. 3); and (b) S_{dist}, where the cost function is only dependent to the distance between consecutive track points (Eq. 4).

$$C = \sum_{n=1}^{n=N-1} \left(\left| V_{n+1} - V_n \right| \right) \quad \text{Eq. 3}$$

$$C = \sum_{n=1}^{n=N-1} d_{n \to n+1} \quad \text{Eq. 4}$$

The second set of sensitivity experiments relates with the constraint that the relative vorticity between consecutive track points may not vary by more than 50% (Section 2.2) and it is composed by three tests, where the 50% threshold has been modified to 25% ($S_{25\%}$), 75% ($S_{75\%}$), 100% ($S_{100\%}$). In all three tests we used the original cost function (Eq. 2) and the identified cyclones from *filter3.*We focused on

filter3 since this is the dataset with the highest number of identified cyclones (Fig. 6), amplifying thus the differences between the tracking results of the sensitivity tests.

Figure 10 presents the lifetime of tracks (i.e. the number of track points) and their average speed (i.e., distance between the track points) for both sets of sensitivity experiments. The results of the first set of experiments that focus on the cost function (Figs 10a and 10b), show that the cyclones lifetime and average speed is quasi-equal for all *filter3*, S_{rel} and S_{dist} (maximum differences are less than 1%). This suggests that the lifetime of track points and their average speed are rather insensitive to the change of the cost function. This is due to the fact that the algorithm always presented several alternative tracks for a single cyclone but in the majority of the cases, these alternative tracks were similar and only presented small deviations from the cyclones' main path. In such cases, the usefulness of the cost function is on choosing the smoothest track in terms of intensity and distance between consecutive track points. It is noteworthy that in S_{rel} and S_{dist}, the algorithm was still bounded by the constraint of linking cyclone centers that presented relative vorticity values that did not vary by more than 50%. Climatologically, the term ***d*** in the cost function does not change significantly the results of the algorithm. However, this term was shown to play an important role, especially when several cyclones of quasi-equal vorticity were located within the 10°x5° area but unrealistically far from the tracked center.

The results of the second set of experiments that relate with the 50% threshold (Figures 10c and 10d) reveal similar distributions for all varying thresholds, however when comparing $S_{100\%}$ and $S_{25\%}$, the former tends to form longer tracks (Fig. 10c) with longer distances between the track points (Fig. 10d). Indeed, when applying smaller (higher) thresholds on the permitted evolution of the cyclones intensity, then it is more likely that the algorithm will form shorter (longer) tracks due to the smaller (higher) accepted differences on the relative vorticity evolution of consecutive track points. Ideally, the 50% threshold could be neglected. However, this would create numerous alternative tracks in the cases of high resolution datasets. In general, the constraints applied in Step-II (i.e. 50% threshold, searching cyclones within a 10°x5° area and the angle criterion; Section 2.2) have been found as a fair

compromise between cutting off “unnatural” candidate cyclone tracks and providing all possible tracks for the algorithm to depict the “correct” one according to the cost function.

3.3 Physical coherence of the tracked cyclones

In this section we perform an analysis of the effective area diagnostic tool described in section 2.1.3, taking into account only *filter5* results. Figure 11 presents the composite life cycle of the cyclones physical characteristics, centered on the time of the maximum vorticity of the tracks (mature stage) and averaged for all tracks detected in the Pacific Ocean (from 130° to 240° of longitude and from 30° to 90° of latitude), North Atlantic Ocean (from 300° to 360° of longitude and from 30° to 90° of latitude) and within the Mediterranean region (from 345° to 45° of longitude and from 25° to 50° of latitude). The results show that regardless of the region, there is a strong coherence between the life cycle of sea level pressure minima, relative vorticity and maximum 10-meter wind speed. Cyclones tend to intensify rapidly but weaken in a slower rate. For the construction of the composites there is no distinction on the cyclones' lifetime. Also, we should note that the further we get from the time of the cyclone’s maximum vorticity (i.e. the composite center) the fewer cyclones last long enough to provide diagnostics for the composites. For example, the Mediterranean cyclones lifetime scale is inferior from the other extra-tropical cyclones and rarely exceeds 2-3 days. Nevertheless, our motivation here is to assess the validity of the effective area diagnostic which seems to capture correctly the physical characteristics of the life cycle of cyclones regardless the region. Indeed, in agreement with Campa and Wernli (2012), we found that Mediterranean cyclones are less deep, in terms of sea level pressure, while Atlantic cyclones are slightly deeper than those occurring over the Pacific Ocean.

4. Conclusions

In this article we presented a new algorithm for identifying and tracking cyclones, applied on winter extra-tropical cyclonic systems over the northern hemisphere. We tested our algorithm's performance for different filtering strengths applied on the high frequency relative vorticity fields. Results showed that the number of tracks were inversely proportional to the filter strength while the cyclone spatial and temporal variability were coherent with those produced by other tracking algorithms presented in the literature. Finally, our algorithm successfully captured the physical characteristics of cyclones.

Our identification and tracking algorithm uses as few constraints as possible, not only for tracking weak vorticity perturbations which evolved in strong cyclones, but also for tracking weak perturbations that did not evolve into strong cyclones. This allows the assessment of the algorithm’s sensitivity to data filtering, but also in the future, a more precise description of the environmental conditions which favor cyclogenesis and cyclone intensification. Furthermore, we chose the vorticity criteria to vary dynamically (vorticity must not vary more than 50% in consecutive time steps) and we avoided any threshold or cut-off values. It should be noted that although we applied our algorithm based on relative vorticity to identify and track cyclones, the same algorithm might be applied on any dataset which presents enclosed areas after applying a threshold value. For instance, our algorithm could be applied for tracking supercells or mesoscale convective systems using datasets of brightness temperature or cloud cover.

Our tracking approach is based on minimizing a cost function of vorticity maxima. We observed some mistakes, especially when cyclonic circulations were found to be very noisy with multiple local maxima. As an alternative cost function, it would be interesting to explore the weighted mean differences of additional cyclone physical characteristics (pressure, wind speed etc.) between consecutive time steps. This has been previously applied by Machado et al. (1998) for tracking MCS based on brightness temperature satellite observations. However, their method assumes a-priori choice of the weighting value, risking restraining our method adaptability to track cyclones of different origin (e.g. extra-tropical and tropical cyclones). Our algorithm links cyclone centers in consecutive time steps, in contrast with the alternative configuration proposed by Machado et al (1998) and Inatsu (2009) to link enclosed areas. This decision was made because large cyclonic circulations would not

correspond to a single cyclone if enclosed areas were linked, and additional criteria -and/or filtering- would be needed, while weak cyclones would be neglected.

Further development of our algorithm includes the extension of the identification part in three dimensions and the extension of the method adaptability for different atmospheric features such as MCS. CycloTRACK was implemented in MatLab and its source code is freely available upon request to the corresponding author.

Acknowledgements

EF was supported by the IMPACT2C program (funded by the European Union Seventh Framework Programme, FP7/2007- 2013 under the grant agreement 282746) and this work has been conducted in the Institut Pierre Simon Laplace group for regional climate and environment studies. The authors are grateful to Philippe Drobinski and Heini Wernli for fruitful discussions on the algorithm configuration, and to Christoph Raible for his help in plotting the cyclone centers density field.

References

Allen, J.T., Pezza, A.B., and Black, M.T.: Explosive cyclogenesis: a global climatology comparing multiple reanalyses, J. Climate, 23, doi: 10.1175/2010JCLI3437.1, 2010.

Blender, R., Fraedrich, K., and Lunkeit, F.: Identification of cyclone-track regimes in the north atlantic., *Quart. J. Royal Meteor. Soc*., 123, doi: 10.1002/qj.49712353910, 1997.

Blender, R., and Schubert, M.: Cyclone Tracking in Different Spatial and Temporal Resolutions, *Mon. Wea. Rev.*, 128, 377–384, 2000.

Čampa, J., and Wernli, H.: A PV Perspective on the Vertical Structure of Mature Midlatitude Cyclones in the Northern Hemisphere, *J. Atmos. Sci.*, **69**, DOI: 10.1175/JAS-D-11-050.1 , 2012.

Campins, J., Genoves, A., Picornell, M.A., and Jansa, A.: Climatology of Mediterranean cyclones using the ERA-40 dataset, *Int. J. Climatol*, 31, doi:10.1002/joc.2183, 2011.

Davis, C.A., Snyder, C., and Didlake, A.: A vortex-based perspective of eastern Pacific tropical cyclone formation, *Mon. Wea. Rev.*, 136, DOI: 10.1175/2007MWR2317.1, 2008

Eckhardt, S., Stohl, A., Wernli, H., James, P., Forster, C., and Spichtinger, N.: A 15-Year Climatology of Warm Conveyor Belts, *J. Climate*, 17, 218–237, 2004.

Flaounas, E., Janicot, S., Bastin, S., Roca, R., and Mohino, E.: The role of the Indian monsoon onset in the West African monsoon onset: observations and AGCM nudged simulations, *Climate Dynamics*, 38, doi: 10.1007/s00382-011-1045-x, 2012.

Flaounas, E., Drobinski, P., and Bastin, S.: Dynamical dowscaling of IPSL-CM5 CMIP5 historical simulations over the Mediterranean: Benefits on the representation of regional surface winds and cyclogenesis, *Clim. Dyn.*, doi: 10.1007/s00382-012-1606-7, 2013.

Hanley, J., and Caballero, R.: Objective identification and tracking of multicentre cyclones in the ERA-Interim reanalysis dataset, *Q. J. R. Meteorol. Soc*., 138, doi:10.1002/qj.948, 2012.

Hewson, T.D., and Titley, H.A.: Objective identification, typing and tracking of the complete life-cycles of cyclonic features at high spatial resolution. Met. Apps, 17: 355–381, 2010

Hodges, K.I.: A general method for tracking analysis and its application to meteorological data, Mon Wea Rev, 122, 2573–2586, 1994

Hodges, K.I.: Feature tracking on the unit sphere, Mon Wea Rev, 123, 3458–3465, 1995.

Hodges, K.I., Adaptive constraints for feature tracking, *Mon. Wea. Rev.*, 127, 1362–1373, 1999.

Hoskins, B.J., and Hodges, K.I.: New perspectives on the Northern Hemisphere winter storm tracks, *Journal of Atmospheric Science* 59, 1041–1061, 2002.

Inatsu, M.: The neighbor enclosed area tracking algorithm for extratropical wintertime cyclones. *Atmosph. Sci. Lett.*, 10, doi: 10.1002/asl.238, 2009.

Kew, S.F., Sprenger M., and Davies H.C, Potential vorticity anomalies of the lowermost stratosphere: A 10-yr winter climatology, *Mon. Wea. Rev.*, **138**, 1234–1249, 2010.

Lagouvardos, K., Kotroni, V., and Defer E.: The 21-22 January 2004 explosive cyclogenesis over the Aegean Sea: observations and model analysis, *Quarterly Journal of Royal Meteorological Society*, 133, doi: 10.1002/qj.121, 2007.

Lim, E.P., and Simmonds, I.: Southern Hemisphere Winter Extratropical Cyclone Characteristics and Vertical Organization Observed with the ERA-40 Data in 1979–2001, *J. Climate*, **20**, 2675–2690, 2007.

Limbach S., Schömer E., and Wernli H., Detection, tracking and event localization of jet stream features in 4-D atmospheric data, Geosci. Model Dev., 5, 457-470, 2012

Machado, L.A.T., Rossow, W.B., Guedes, R.L., and Walker, A.W.: Life Cycle Variations of Mesoscale Convective Systems over the Americas, *Mon. Wea. Rev*, 126, 1630–1654, 1998.

Murray, R.J., and Simmonds, I.: A numerical scheme for tracking cyclone centres from digital data. Part I: Development and operation of the scheme, Austr. Meteorol. Mag, 39, 155–166, 1991.

Neu, U., and Coauthors: IMILAST: A Community Effort to Intercompare Extratropical Cyclone Detection and Tracking Algorithms, *Bull. Amer. Meteor. Soc.*, **94**, 529–547, 2013.

Nissen, K.M., Leckebusch, G.C., Pinto, J.G., Renggli, D., Ulbrich, S., and Ulbrich, U.: Cyclones causing wind storms in the Mediterranean: Characteristics, trends and links to large-scale patterns, *Nat. Hazards Earth Syst. Sci.*, 10, doi:10.5194/nhess-10-1379-2010, 2010.

Pinto, J.G., Spangehl, T., Ulbrich, U., and Speth, P.: Sensitivities of a cyclone detection and tracking algorithm: individual tracks and climatology, Meteorol Z, 14, 823–838, 2005.

Raible, C.C., Della-Marta, P.M., Schwierz, C., Wernli, H., and Blender, R.,: Northern Hemisphere Extratropical Cyclones: A Comparison of Detection and Tracking Methods and Different Reanalyses. *Mon. Wea. Rev.*, **136**, 880–897, 2008

Roca, R., Lafore, J.P., Piriou, C., and Redelsperger, J.L.: Extratropical Dry-Air Intrusions into the West African Monsoon Midtroposphere: An Important Factor for the Convective Activity over the Sahel, *J. Atmos. Sci*, 62, 390–407, 2005.

Sanders, F., and Gyakum, J.R.: Synoptic-dynamic climatology of the ‘bomb’, *Mon. Wea. Rev.*, **108,** 1589–1606, 1980.

Satake, Y., Inatsu, M., Mori, M., Hasegawa, A.: Tropical Cyclone Tracking Using a Neighbor Enclosed Area Tracking Algorithm. *Mon. Wea. Rev.*, 141, 3539–3555, 2013

Serreze M., Carse, F., Barry, R., and Rogers, J.: Icelandic low cyclone activity: climatological features, linkages with the NAO, and relationships with recent changes in the Northern Hemisphere circulation, Journal of Climate, 10(3), 453–464, 1997.

Sinclair, M.R.: An Objective Cyclone Climatology for the Southern Hemisphere. *Mon. Wea. Rev.*, **122**, 2239–2256, 1994

546

547 Sinclair, M.R.: Objective Identification of Cyclones and Their Circulation Intensity, and Climatology.
548 *Wea. Forecasting*, **12**, 595–612, 1997

549

550 Trigo, I., Davies, T., and Bigg, G.: Objective climatology of cyclones in the Mediterranean region,
551 Journal of Climate 12(6): 1685–1696, 1999.

552

553 Trigo, I.F.: Climatology and interannual variability of stormtracks in the Euro-Atlantic sector: a
554 comparison between ERA-40 and NCEP/NCAR reanalyses, Clim Dyn, 26, 127–143, 2006.

555

556 Wernli, H., and Schwierz, C.: Surface cyclones in the ERA-40 dataset, part I, novel identification
557 method and flobal climatology, J Atmos Sci, 63:2486–2507, 2006.

558

559 Wernli, H., and Sprenger, M.: Identification and ERA-15 climatology of potential vorticity streamers
560 and cutoffs near the extratropical tropopause, *J. Atmos. Sci.*, 64, 1569–1586, 2007.

561

562 Ulbrich, U., Leckebusch, G.C., and Pinto, J.G.: Extra-tropical cyclones in the present and future
563 climate: a review, *Theoretical and Applied Climatology.*, 96, doi: 10.1007/s00704-008-0083-8, 2009.

564

565 Ulbrich, U. and co-authors: Are Greenhouse Gas signals of Northern Hemisphere winter extra-tropical
566 cyclone activity dependent on the identification and tracking methodology?, Meteorol Z,

567 22, doi:10.1127/0941-2948/2013/0420, 2013.

Uppala, S., Dee D., Kobayashi, S., Berrisford, P., and Simmons, A.: Towards a climate data assimilation system: status update of ERA-interim, ECMWF Newsletter, 115, 12–18, 2008.

Figure captions

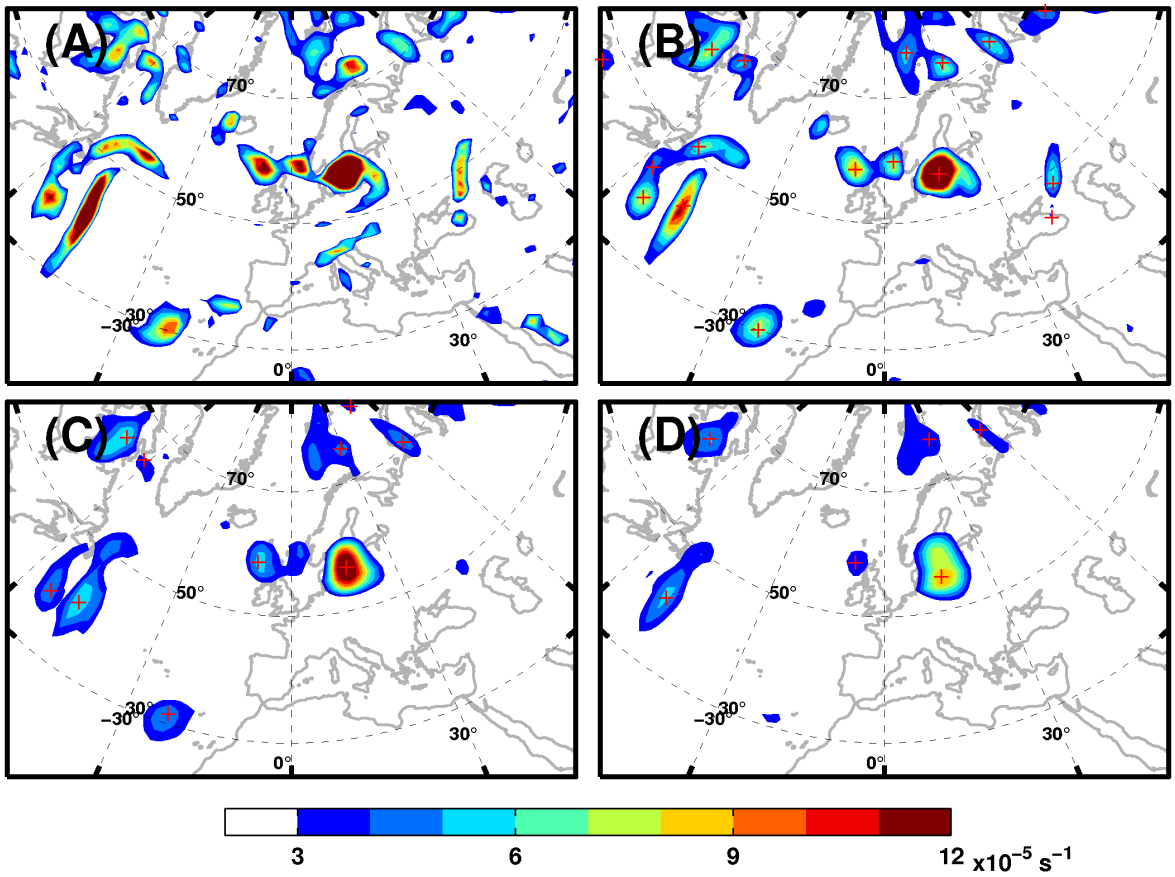

Figure 1 (A) Relative vorticity raw fields at 00:00 UTC, 3 December 1999. The applied threshold is $3x10^{-5}$ s^{-1}. Crosses represent central maxima located in the center of a 3x3 grid point area. (B) as in (A) but relative vorticity field is filtered using a 3x3 correlation spatial filter. (C) as in (A) but relative vorticity field is filtered using a 5x5 correlation spatial filter. (D) as in (A) but relative vorticity field is filtered using a 7x7 correlation spatial filter.

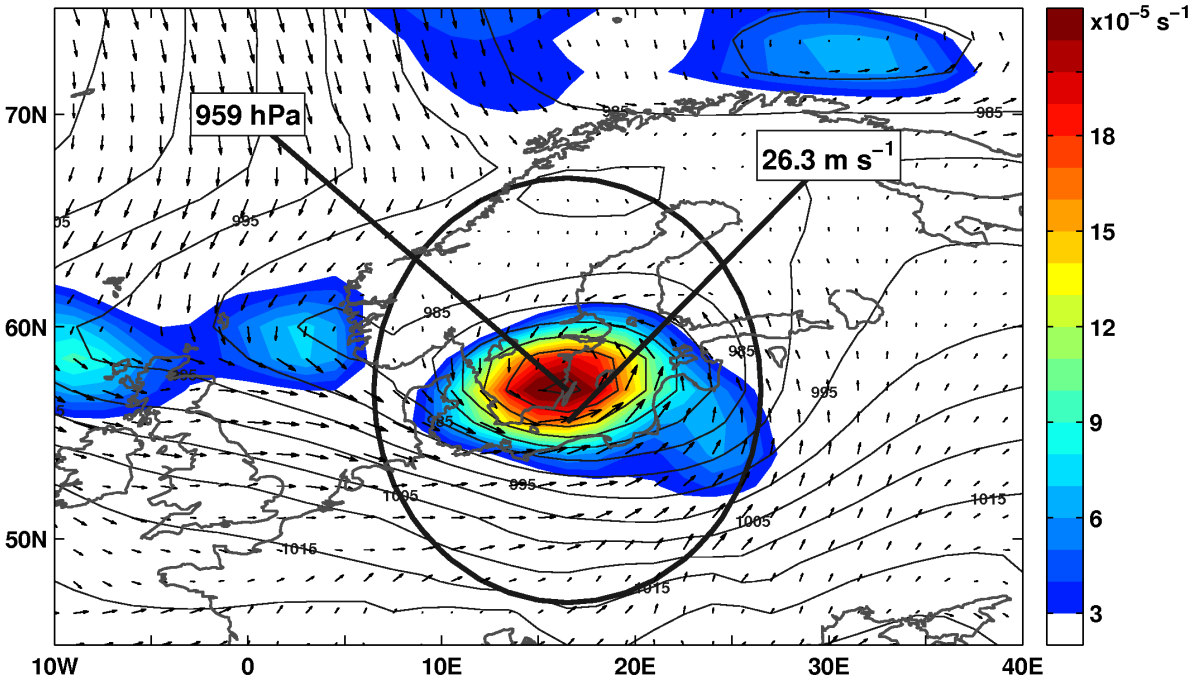

Figure 2 The Anatol storm at 00:00 UTC, 3 December 1999. Relative vorticity is smoothed by a 3x3 spatial filtering (*color*); the contour denotes the mean sea level pressure; and arrows denote 10-meter wind field. Thick black contour represents the effective area of the cyclone. Locations and values of maximum wind speed and lower sea level pressure is depicted by the thick lines.

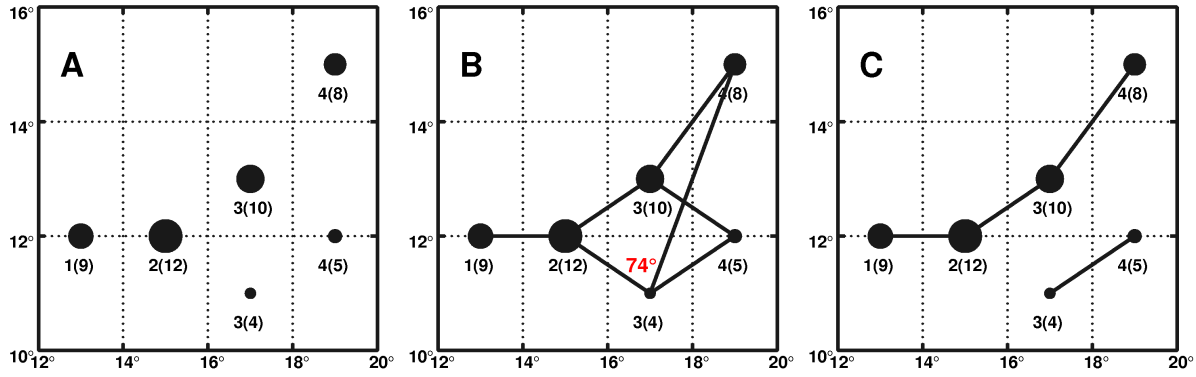

Figure 3 (A) An idealized case of cyclone locations in four time steps. The locations are depicted by *circles*. The numbers above the locations are in the form X(Y), where *X* denotes the time step and *Y* denotes the relative vorticity. The circle sizes are proportional to the relative vorticity value of the cyclone. (B) all possible trajectories of cyclone 2(12) by searching backwards and forward in time. (C) A selected subset of tracks of (B): we retain those which present the minimum average change of relative vorticity in successive time steps.

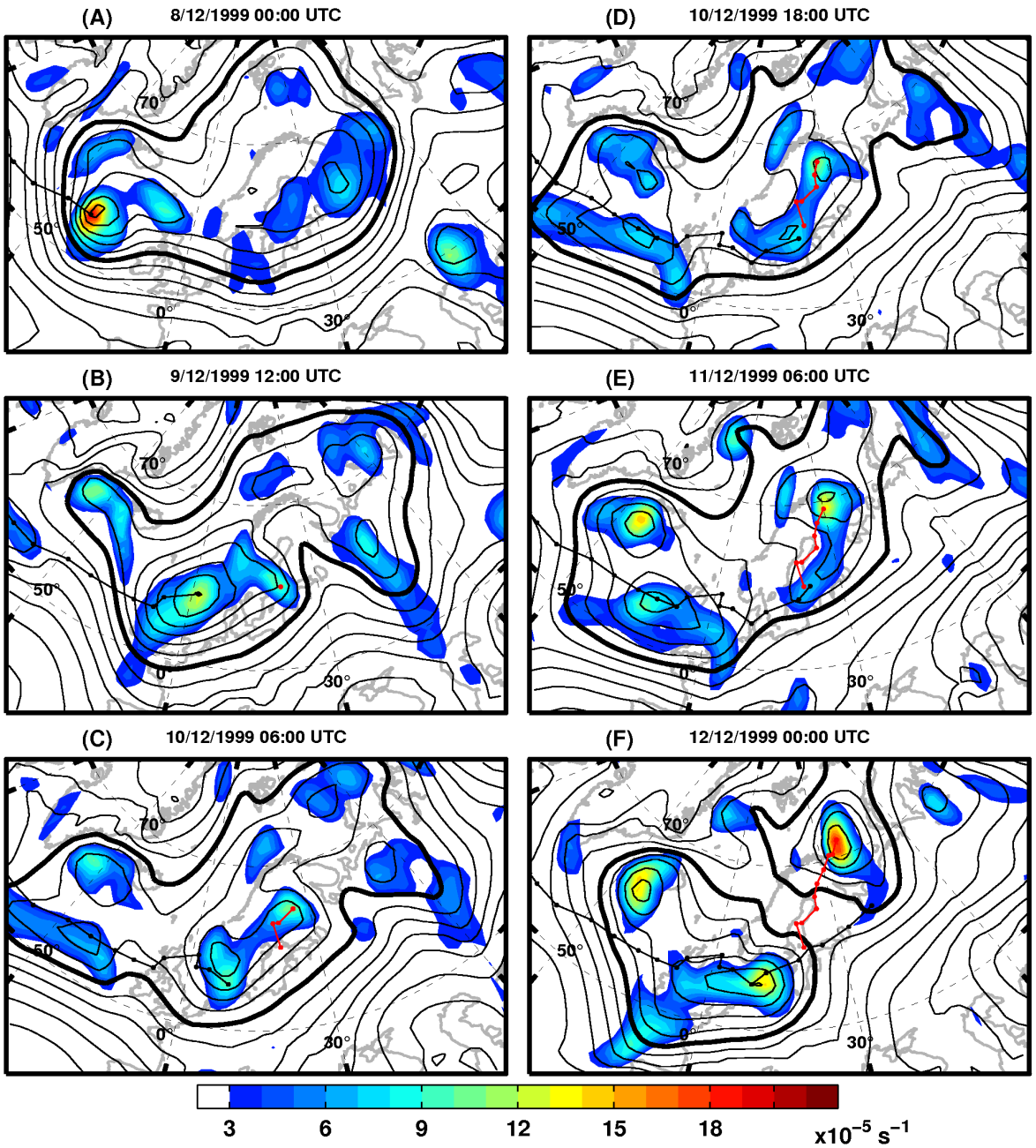

600

601 Figure 4 Relative vorticity smoothed by a 3x3 spatial filter (*color*); sea level pressure (*contours*, with a
602 5 hPa interval, thick contour denotes 1000hPa); and tracks (thin lines) of two splitting cyclones for
603 different times during December 1999.

604

605

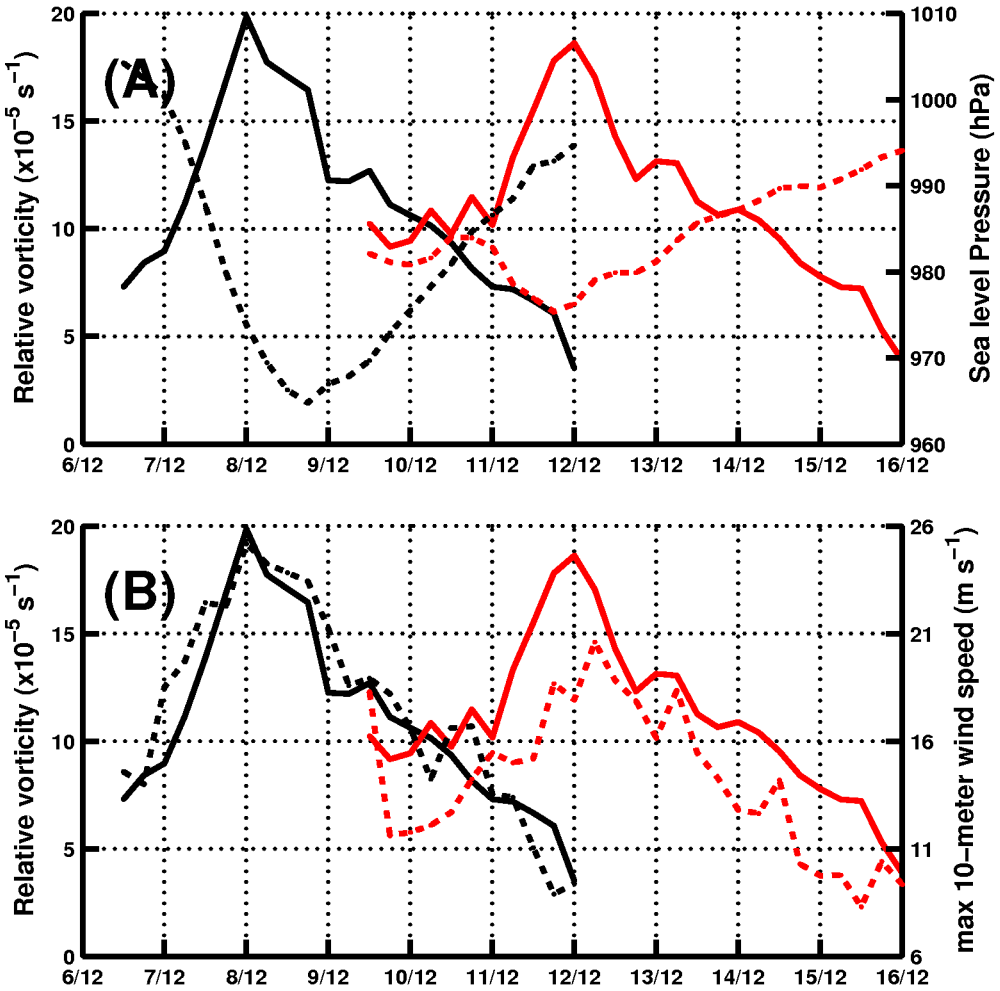

606

607 Figure 5 (A) Maximum relative vorticity (solid line) at the track centers and minimum sea level
608 pressure (dashed line) as detected within the cyclones effective area for the two cyclones shown in Fig.
609 4. (B) as in (A) but dashed line corresponds to maximum 10-meter wind speed. Color lines are the
610 same as in the tracks in Fig. 4. The horizontal axes represent the period 6-16 December 1999.

611

612

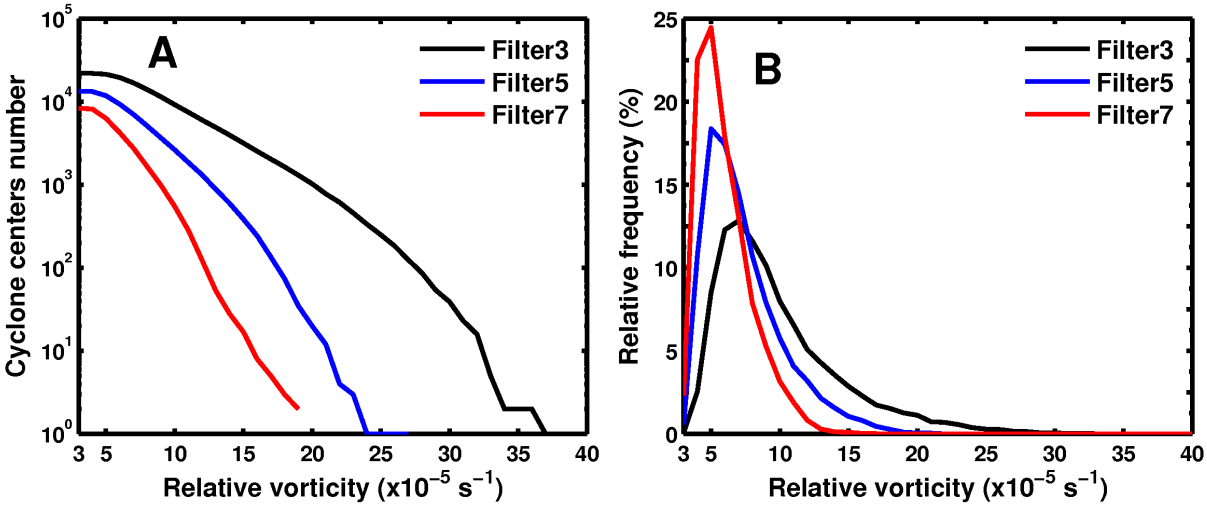

613

614 Figure 6 (A) The number of cyclonic centers as function of their relative vorticity and as detected by
615 the three algorithm sensitivity tests. (B) Relative frequency distributions as a function of the relative
616 vorticity for the identified cyclone centers.

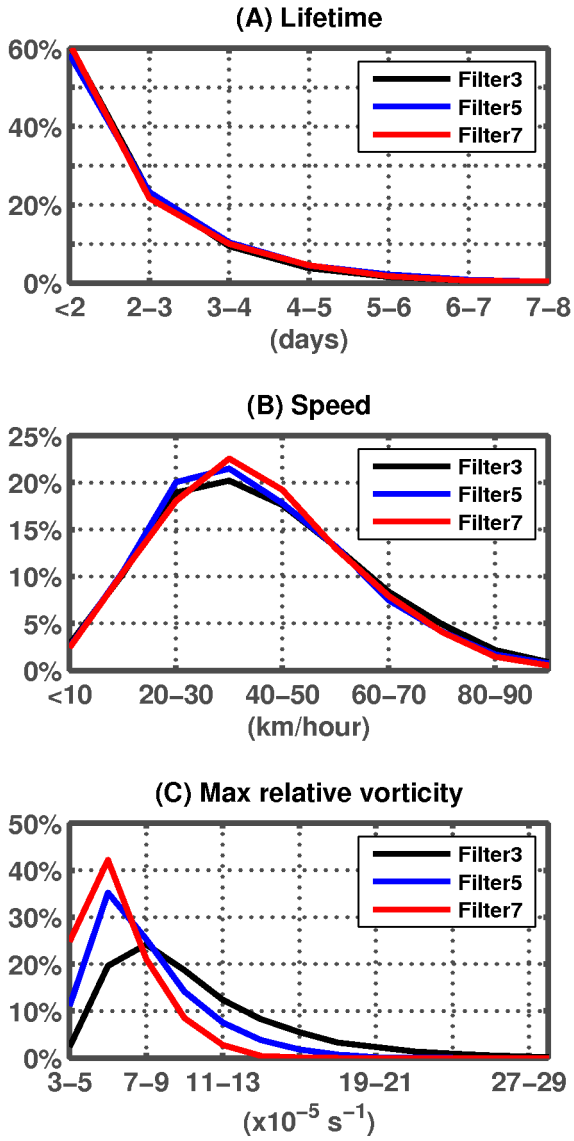

617

618 Figure 7 (A) Relative frequency distributions of cyclones lifetimes for the three sensitivity tests. (B)

619 As in (A) but for cyclones average speed. (C) as in (A) but for tracks maximum relative vorticity.

620

621

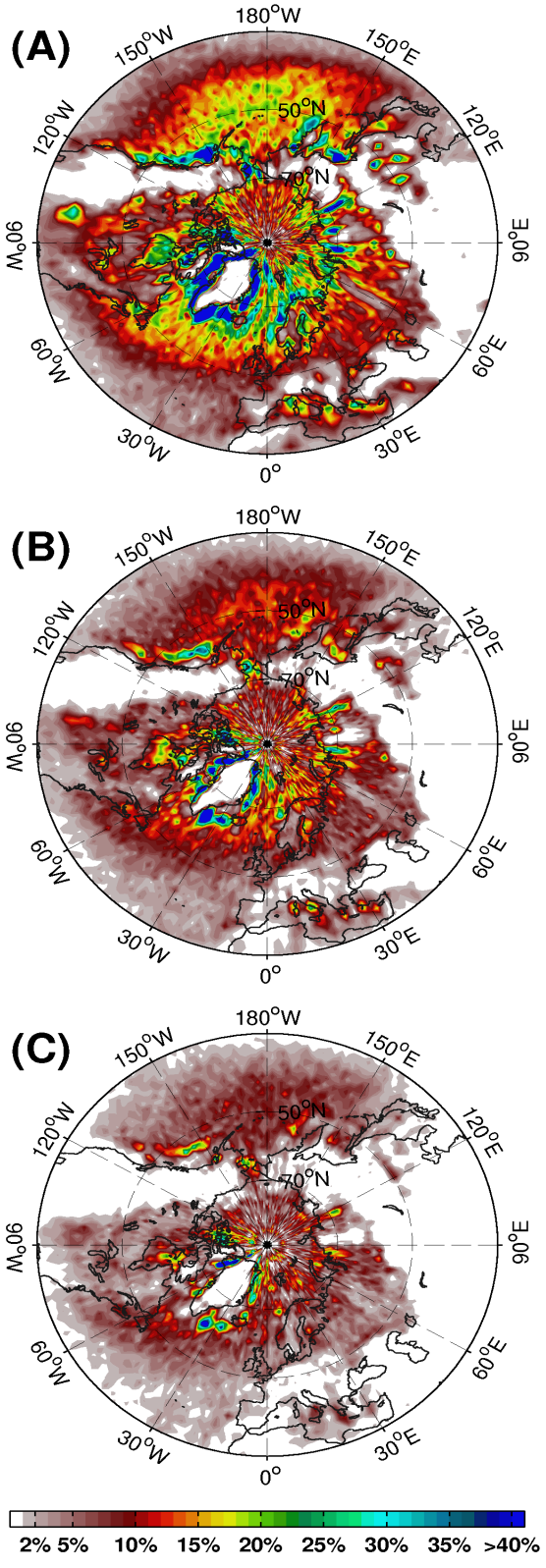

622

623 Figure 8 Cyclone center density expressed as the percentage of cyclone occurrence per time step and

624 per unit area of 1000 km^2 for: (A) *filter3;* (B) *filter5*; and (C) *filter7*.

625

626

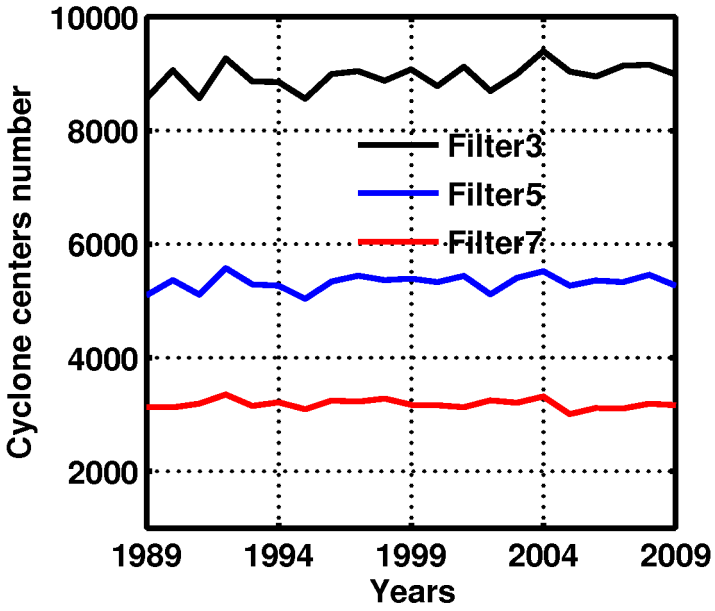

627

628 Figure 9 The number of cyclone centers per year for the three sensitivity tests.

629

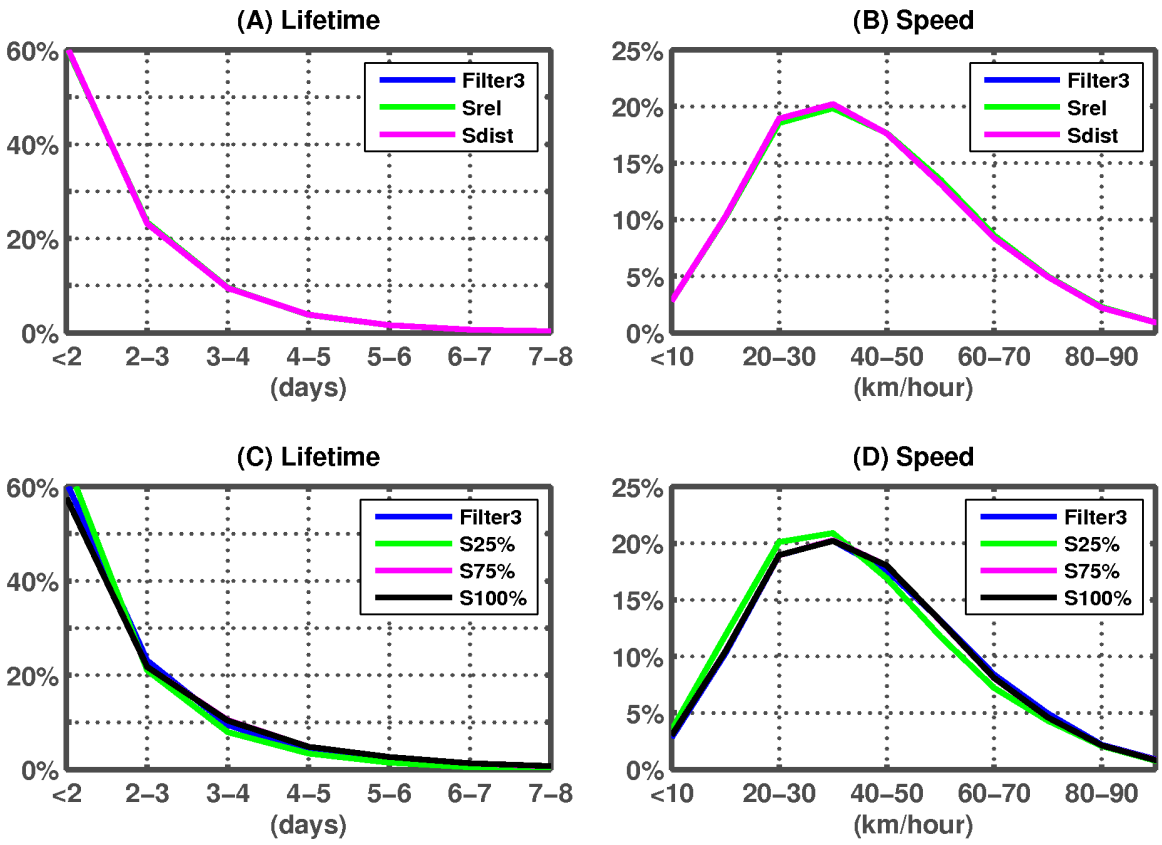

630

631 Figure 10 (A) Relative frequency distribution of cyclones' lifetime for the sensitivity tests *filter3*, S_{rel}

632 and S_{dist}. (B) As in (A) but for cyclones average speed. (C) As in (A) but for the sensitivity tests *filter3*,

633 $S_{25\%}$, $S_{75\%}$ and $S_{100\%}$. (D) as in (B) but for the sensitivity tests *filter3*, $S_{25\%}$, $S_{75\%}$ and $S_{100\%}$

634

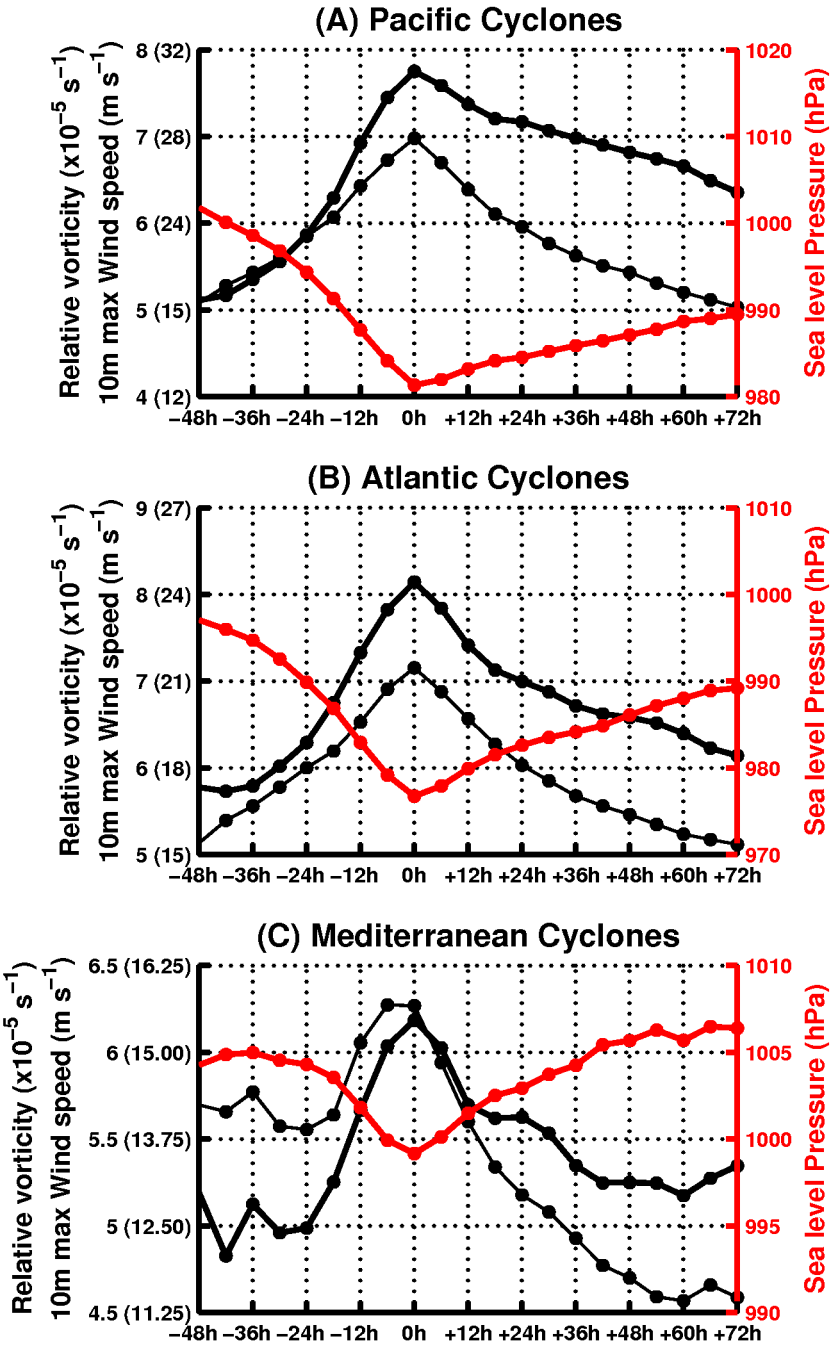

Figure 11 (A) Average composite time series of Pacific cyclones physical characteristics. “0h” corresponds to the time that the cyclone presents its maximum relative vorticity. We denote relative vorticity (thick black line), sea level pressure (red thick line) and maximum 10-meter wind speed (thin black line). Wind speed scale values are shown in the left vertical axes in parenthesis. (B) as in (A) for the Atlantic cyclones. (C) as in (A) for Mediterranean cyclones. Note that Y-axis has not the same value intervals across the three panels.